ORIGINAL ARTICLE

Boundary lubrication with aqueous solutions of silicone-based amphiphilic block copolymer aggregates: effect of concentration

Hikaru Kimura[1] · Takumi Miyamoto[1] · Naoyuki Yamazaki[2] · Shunichi Watanabe[2] · Shinji Yamada [1]

Abstract

The thin film structures and tribological properties of aqueous solutions of a silicone-based amphiphilic block copolymer, bis-isobutyl polyethylene glycol (PEG)-14/amodimethicone (BIPA) copolymer, confined between mica surfaces were investigated using the surface forces apparatus. Measurements were made for three BIPA concentrations (0.005, 0.05, and 0.5 wt%); the effect of concentration on the structures and properties was evaluated. The BIPA molecules had positive charges in the solutions and formed an adsorbed layer on a negatively charged mica surface. The static hard-wall thicknesses were within the range of 3.3–5.6 nm for the three concentrations. Applying sliding motions under load L further decreased the thickness. The minimum dynamic thicknesses were 2.4–2.7 nm for the three concentrations, indicative of sliding between two adsorbed BIPA molecular layers. The friction coefficients were on the order of 10^{-5} for the three concentrations; extremely low friction was obtained originating from the slippage of the fluid-like water layer between the adsorbed layers. All three concentrations exhibited good lubricity, but precise comparison implies some differences in the film structures and friction mechanisms. The details of the differences were discussed from the perspective of the dissolution states of BIPA in the solutions and adsorbed/sliding conformations.

Introduction

The friction properties between two opposed surfaces separated by a molecularly confined lubricant fluid are very different when comparing aqueous (water-based) and oil-based lubrication systems. When a lubricant fluid is confined in a nanometer-scale gap between surfaces, the fluid molecules are geometrically packed, which induces an increase in the density of the fluid. Regarding oils, the density increase directly leads to an increase in the fluid viscosity. A number of experiments using the surface forces apparatus (SFA) [1–6] and computer simulations [7] observed an extensive increase in the fluid viscosity in confinement, and solid-like shear behaviors for many different lubricant oils were observed. On the other hand, in

the case of water, the structure and dynamics in molecular-scale confinement are totally different from those of oils. Because of the strong orientation dependence of the hydrogen bonds, the density of liquid water is higher than that of solid ice. Therefore, geometrical confinement and the resulting density increase do not induce solidification of water, and the system still has high fluidity [8]; this is the essential mechanism for the extremely low friction of aqueous lubrication systems. Biological sliding systems, such as articular cartilage, organs in our body, and eyelids, are representative examples of low friction based on the aqueous lubrication mechanism [8–13].

Although aqueous lubrication often realizes extremely low friction, water itself is not a good lubricant under boundary conditions. Water has high fluidity even in molecular-scale confinement, as was already mentioned. This means that water molecules tend to be squeezed out easily from the contact interface under an applied load (low load-carrying capacity). Therefore, appropriate water-soluble materials must be used as additives to obtain good aqueous lubrication. Water-soluble additives have functional groups, such as charged or polar groups, in the molecules. The water molecules adjacent to such groups form hydration shells that produce short-range repulsive

✉ Shinji Yamada
  yamada.s@kao.com

1   R&D—Analytical Science Research, Kao Corporation, Wakayama, Japan

2   R&D—Hair Care Products Research, Kao Corporation, Tokyo, Japan

force [8, 14–16]. If the additive molecules are confined between or adsorbed onto surfaces, the repulsive force supports normal load and prevents water molecules from being squeezed out from the interface. This is the molecular origin of the load-carrying capacity of aqueous lubrication. The relaxation time of water molecules in the hydration shells is on the order of nanoseconds, only 10^2 times longer than that in bulk water [8, 17]. This short relaxation time realizes fluid-like sliding of the water layer even in molecular-scale confinement and results in extremely low friction. The details of the aqueous lubrication behaviors have been published for many different systems: salt solutions [15, 18, 19], polymer brushes [20–22], amphiphilic surfactant layers [14, 23, 24], liposomes [24, 25], and biological molecules/biomaterials [26–32].

In our earlier work [33], we demonstrated a new class of aqueous lubrication systems that give extremely low friction: a dilute solution of amphiphilic block copolymer aggregates. The tribological properties were investigated for the aqueous solution of a silicone-based amphiphilic block copolymer, bis-isobutyl PEG-14/amodimethicone (INCI name, henceforth referred to as BIPA) copolymer (concentration of 0.05 wt%), confined between mica surfaces using the SFA. BIPA molecules existed as positively charged water-soluble aggregates in the solution and formed an adsorbed layer on negatively charged mica surfaces. AFM observations and SFA normal force measurements suggested the deposition of aggregates on the top of the adsorbed layer. When the two surfaces were compressed by a normal load and sliding motions were applied between the surfaces, most of the deposited aggregates were squeezed out from the sliding interface, and extremely low friction was obtained. The friction coefficient μ was on the order of 10^{-5}, which is almost equivalent to the lowest μ values reported in the literature of comparable SFA studies [8].

In this work, we examined the thin film structures and tribological properties of BIPA aqueous solutions with different BIPA concentrations. The effects of concentration on the structures and properties are important from the viewpoint of practical applications [34]. AFM and SFA measurements were made for the BIPA solutions at three concentrations (0.005, 0.05, and 0.5 wt%). The results showed that sliding films of two adsorbed layers were obtained for the three concentrations, with μ values on the order of 10^{-5}. All three concentrations exhibited excellent friction reduction ability, but a detailed comparison implied some differences in the sliding structures and friction properties depending on the concentrations. The molecular-scale mechanisms of the differences were discussed from the perspective of the dissolution states of BIPA in the solutions (unimers or aggregates) and resulting adsorbed/sliding conformations.
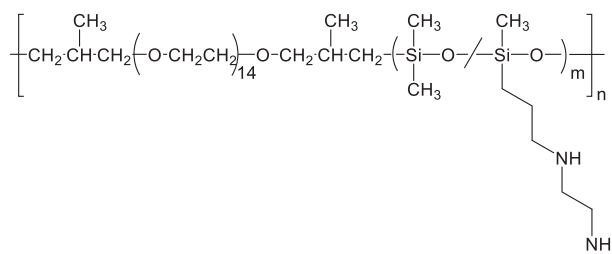

Fig. 1 Chemical structure of bis-isobutyl PEG-14/amodimethicone (BIPA) copolymer

Experimental section

Materials

A silicone-based amphiphilic block copolymer, BIPA (Fig. 1), was purchased from Dow Corning Toray Silicone Co., Ltd. (Tokyo, Japan) and used as received. The chemical structure and impurities included in the sample were analyzed using gel permeation chromatography (GPC) and ^{1}H NMR, which were described in detail in our previous publication [33]. The modification ratio of the amino-modified siloxane segment was ~5%. The degree of polymerization (DP) of the siloxane segments (m in Fig. 1) was ~16, and the DP of the whole backbone segments (n in Fig. 1) was ~5. The M_w of the polymer was ~9100 (calibrated with standard polystyrene samples), and the polydispersity index (M_w/M_n) was ~1.6. The polymer included two major impurities: dimethyl, (aminoethylaminopropyl) methyl cycrosiloxanes and PEG-type components. Aqueous solutions at three concentrations (0.005, 0.05, and 0.5 wt%) were prepared by dissolving BIPA copolymer into ultrapure water, which was purified by a Direct-Q® UV water purification system (Merck Millipore, MA, USA). No salt was added to the BIPA solutions. The solutions with concentrations of 0.005 and 0.05 wt% were clear, but that of 0.5 wt% was cloudy.

Atomic force microscope (AFM)

The adsorption behavior of BIPA molecules on mica from solutions was studied by AFM (Dimension XR, Bruker Co., USA) using a triangular silicon nitride cantilever (Bruker ScanAsyst-Fluid+, tip radius: 2 nm, nominal spring constant: 0.7 N/m, resonant frequency: 150 kHz). AFM images were collected in PeakForce Tapping mode® (scan size: 3 × 3 μm). The peak force setpoint was 350 pN, the PeakForce tapping amplitude was set to 100 nm, and the PeakForce tapping frequency was 2 kHz. The AFM images were recorded at a scan rate of 0.5 Hz. The obtained images were processed with the "flatten" function (first order) via built-in software.
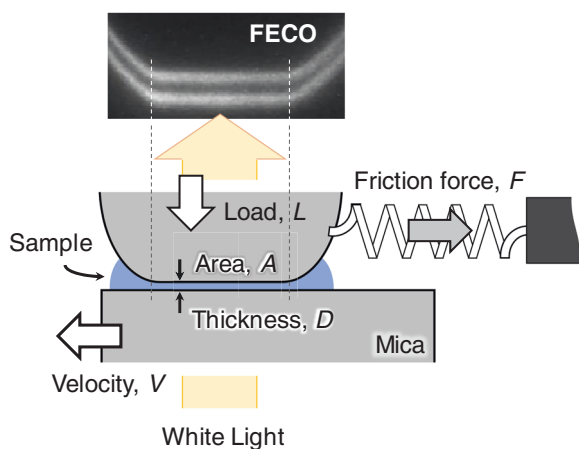
Fig. 2 Schematic illustration of the SFA friction measurement. Droplet of a BIPA copolymer solution is confined between mica surfaces under an applied load L. Lateral motions at a constant sliding velocity V are applied, and the resulting friction force F is measured. Thickness of the sliding film D, size of the contact area A, and the contact geometry are evaluated by observing the FECO fringes during the whole measurement

Surface forces apparatus (SFA)

The surface forces apparatus used in this study was SFA3 (Surforce LLC, CA, USA) [35]. A schematic illustration of a friction measurement is shown in Fig. 2. Molecularly smooth mica surfaces were used as substrates that were aligned in a crossed cylindrical configuration, and a droplet of the BIPA solution (ca. ~0.1 mL) was injected between them. Some amount of water was also placed in the bottom of the chamber to minimize water evaporation from the sample droplet. Regarding friction measurement, surfaces were brought into contact by applying a load, L. The load was controlled by a normal force spring (spring constant of 8380 N/m) of the bimorph slider. The friction force was measured under a given applied load L in the range of ~20 mN (pressure P in the range of ~13 MPa) by applying lateral motions (reversible cycling) to the lower mica surface [36]. The thickness of sliding film D (accuracy within 0.2 nm), size of contact area A, and contact geometry (shape) were evaluated by monitoring fringes of equal chromatic order (FECO). Experiments were performed in a temperature-controlled room ($21 \pm 1\,°C$). We started experiments by measuring the normal force profile; the measurement was started ~20–30 min after the injection of the sample solution between the mica surfaces. After the normal force measurement, the surfaces were separated to a distance of many microns, the two surfaces were brought together and allowed to make contact again (the same contact position as the normal force measurement), and friction measurements were performed. The results reported in this paper are based on at least three independent measurements (three different pairs of mica surfaces).

Results

BIPA adsorption behavior

The adsorption of BIPA molecules onto mica surfaces from solutions was studied using AFM, and the results are shown in Fig. 3. The AFM observation was started ~2 min after dropping the BIPA solution onto the mica surface; it took ~10 min to obtain a $3 \times 3\,\mu m$ image. Scanning started from the top (direction from left to right) in Fig. 3; the surface structures seen near the top represented a very initial stage of BIPA adsorption. For the AFM image of 0.005 wt% (Fig. 3a), we observed a dark flat region only near the top of the image. Evaluation of the surface roughness revealed that the dark flat region was the mica surface without any adsorbates. Most of the rest of the scanned area was covered by an adsorbed layer with a thickness of 1.9 ± 0.1 nm (evaluated from the height difference from the mica surface) and a maximum roughness R_z of 1.2 ± 0.2 nm. A fine "mesh-like" structure was observed in the adsorbed layer, and some bright spots were seen on the top of the adsorbed layer, with a size of ~20 nm. For the 0.05 and 0.5 wt% solutions (Fig. 3b, c), we did not see (time-dependent) different structures within the images. Both images showed a sea-island structure; the size of the island (bright area) was larger at 0.5 wt%. The R_z of the dark "sea" region was 1.7 ± 0.2 nm for 0.05 wt% and 2.2 ± 0.4 nm for 0.5 wt%. The typical lateral size of the island was ~100–200 nm for 0.05 wt% and near 300 nm or larger for 0.5 wt%. The inset images show the structures observed ~15 min after sample preparation. Lateral growth of the island size was seen for all concentrations. For 0.5 wt%, the growth of the island led to the formation of a connected structure; the bright area in the inset image of Fig. 3c constitutes a continuous structure region.

Normal force profiles measured with SFA

The normal force profiles (on approach) for the BIPA solutions at three different concentrations measured using SFA are shown in Fig. 4. Monotonous repulsion was observed for the three concentrations. The surface distance where repulsion started was the smallest for the 0.005 wt% solution, and the distance increased with increasing BIPA concentration. The effect of concentration on the hard-wall distance (where the repulsive force diverges) was not simple; the maximum hard-wall thickness was obtained for 0.05 wt%. The distances where repulsion starts and the hard-wall thicknesses for the three concentrations are summarized in Table 1.

SFA friction measurement

The SFA enabled us to measure the dynamic thicknesses (thicknesses during sliding); the results were plotted as a function of the applied load/pressure and are shown in Fig. 5.
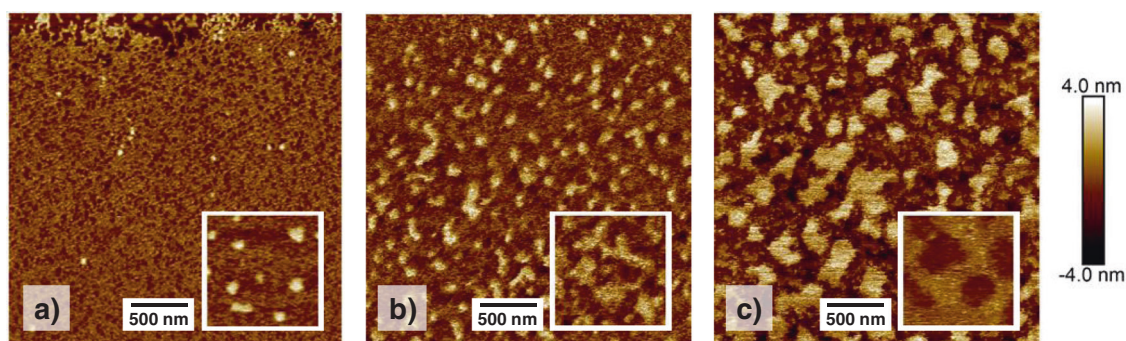
Fig. 3 AFM topographic images of the adsorbed films on mica surfaces from the BIPA solutions with different concentrations. **a** 0.005 wt%, **b** 0.05 wt%, and **c** 0.5 wt%. The three large images were obtained immediately after sample preparation (measurement started ~2 min after sample preparation). The inset images exhibit the surface topography obtained ~15 min after preparation, which show the lateral growth of the island structure. The 500 nm scale bars and the height bar on the right are valid for both the large and inset images
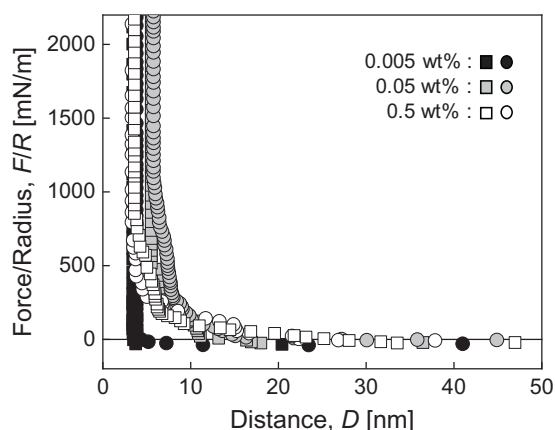

Fig. 4 Normal force profiles (on approach) for the BIPA solutions with three concentrations. The results obtained from two independent measurements are plotted for each concentration

Table 1 Results of the normal force measurements

BIPA concentration [wt%]	Distance where repulsion starts [nm]	Hard-wall thickness [nm]
0.005	4.1 ± 0.5	3.9 ± 0.4
0.05	15.8 ± 1.1	5.6 ± 0.1
0.5	31.2 ± 7.7	3.3 ± 0.5

Regarding the load dependence (Fig. 5a), the dynamic thickness was the largest for sliding at 1 mN (smallest L condition), and increasing L decreased the thickness. When we compare the dynamic thicknesses between concentrations at $L = 1$ mN, the thickness was the smallest (smaller than 4 nm) for 0.005 wt% and the largest (~8 nm) for 0.5 wt%. The minimum dynamic thicknesses under maximum load conditions ($L = 20$ mN) were 2.7 ± 0.1 nm for 0.005 and 0.05
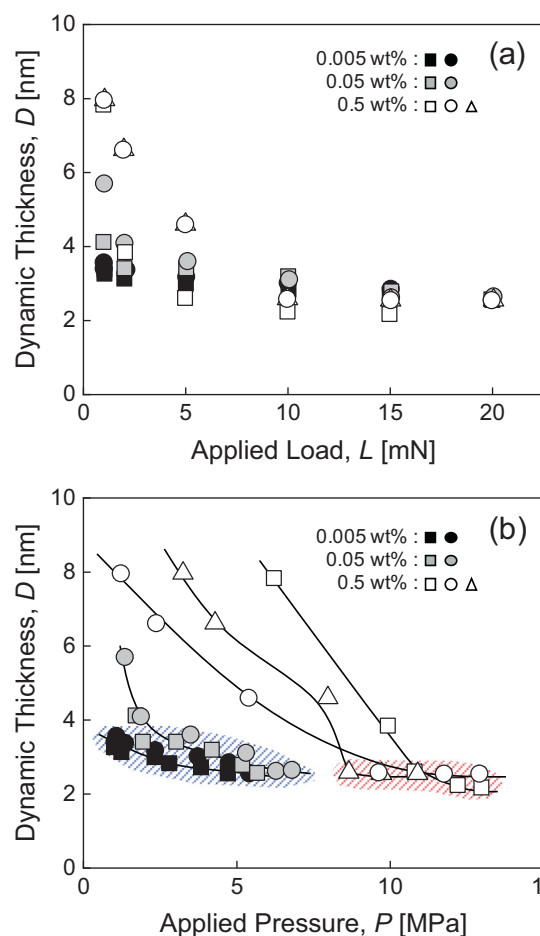

Fig. 5 The dynamic thickness D for the thin BIPA films at three concentrations plotted as a function of applied load L (**a**) and of pressure P ($= L/A$, A: contact area) (**b**). The results obtained from two independent measurements are plotted for 0.005 and 0.05 wt%, and those from three independent measurements are plotted for 0.5 wt%; different symbols represent the data from different (independent) measurements. The sliding velocity V was 0.013 μm/s
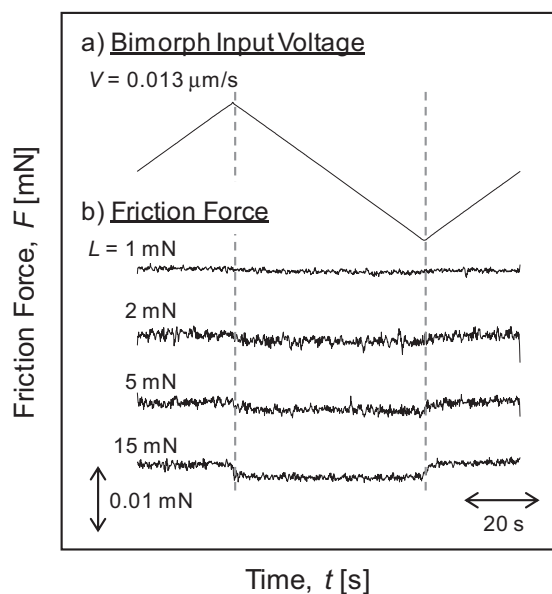
Fig. 6 Typical example of the friction traces for the thin film BIPA solution with a concentration of 0.05 wt%. Triangular voltage signal was inputted to the bimorph slider (**a**) and resulting friction force (**b**) was recorded as a function of time

Fig. 7 Friction force F as a function of the applied load L for the three concentrations (**a**). The same data plotted as the shear stress S ($=F/A$) versus applied pressure P (**b**). Typical FECO fringes for 0.005 wt% and 0.5 wt% are also included. The sliding velocity V was 0.013 μm/s. Symbols correspond to the results shown in Fig. 5

wt% and 2.4 ± 0.2 nm for 0.5 wt%. Figure 5b shows the same dynamic thickness data plotted against the applied pressure P ($=L$/contact area A). It is interesting to note that although the experimental L range was the same (1–20 mN) for the three concentrations, the P range was different. This is due to the fact that the effect of L on A was different between concentrations; the increase of A by the increase of L was relatively small for 0.5 wt% (see also Fig. 8).

Figure 6 shows a typical example of the friction traces (friction force versus time plots) obtained in this study. A triangular voltage signal was applied to the bimorph strips to generate repetitive sliding motions at a constant sliding velocity V (a), and the friction force was detected (b). At $L = 1$ mN, the friction force was too small to be measured in our experimental setting (the detection limit was ~6×10^{-4} mN). When L was increased to 2 mN, a slight friction response was observed, which increased with increasing L.

The friction force was measured as a function of the applied load for the three concentrations, and the result is shown in Fig. 7a. Sometimes the friction force was below the detection limit and could not be measured, which was the case for the low load conditions (≤5 mN) for the 0.5 wt% solution (open squares and open triangles). As shown in the figure, the friction force increased with increasing applied load for the three concentrations. We fit the relationship between F and L by Amontons' law modified for molecular smooth surfaces [1, 2],
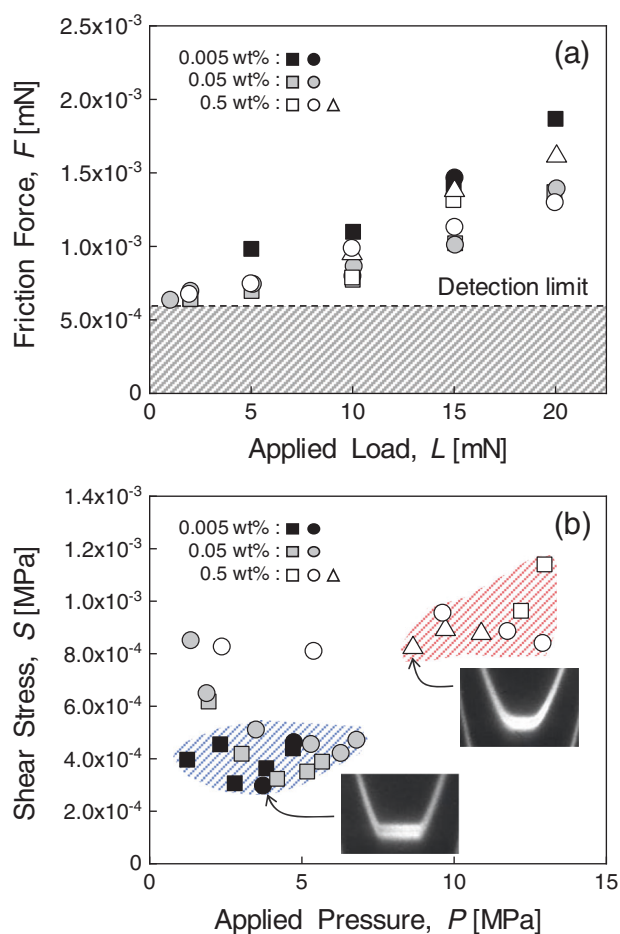
$$F = F_0 + \mu L \tag{1}$$

Table 2 Friction coefficients for the BIPA solutions at three concentrations obtained using Eq. 1

BIPA concentration [wt%]	Friction coefficient μ [$\times 10^{-5}$]
0.005	6.9 ± 1.2
0.05	3.7 ± 0.4
0.5	4.8 ± 0.7

where F_0 is the zero-load friction force (adhesion contribution); the obtained μ values are listed in Table 2. The μ values were on the order of 10^{-5} for the three concentrations, which corresponds to our previous result [33].

The same friction force data were normalized by the contact area A and plotted as the shear stress S ($=F/A$) versus pressure P ($=L/A$), which is shown in Fig. 7b. The distribution of the data points in Fig. 7b is very different from that in Fig. 7a. When we divide both sides of Eq. 1 by

A, we obtain

$$S = \frac{F}{A} = \frac{F_0}{A} + \mu \frac{L}{A} = S_0 + \mu P \qquad (2)$$

For the results of the 0.005 and 0.05 wt% solutions, most of the data points were within the S range of $3–5 \times 10^{-4}$ MPa and did not exhibit a P dependence (blue shaded area in Fig. 7b). This means that for the two concentrations, S is mainly determined by S_0, and μ in Eq. 2 should be nearly zero. On the other hand, for the 0.5 wt% solution, we obtained data points mainly in the large P region, and the S values were within the range of $8–11 \times 10^{-4}$ MPa (red shaded area), which were larger than the two thinner concentrations. Unfortunately, we did not have many data points in the small P region, but the S for small P should be small because many F data points at low L were below the detection limit (as was mentioned). This means that the S-P plot for 0.5 wt% may have a positive slope (finite μ value in Eq. 2). Typical FECO images for 0.005 wt% and 0.5 wt% are included in Fig. 7b. The fringe shape for 0.005 wt% was completely flat at the bottom (thickness of the intervening film was uniform over the entire contact area) and with a sharp edge on both sides. On the other hand, the fringe shape for the 0.5 wt% sample was rather rounded at the bottom, suggesting that the thickness was minimal at the center of the contact area. These different characteristics of the fringe shape imply different contact mechanics models. These analyses suggest different thin film structures and sliding features of the thin BIPA films depending on the concentrations, and this phenomena will be discussed in the following section.

Discussion

General trends of thin film structures and friction properties

According to our previous study on BIPA solution with a concentration of 0.05 wt% [33], BIPA molecules form amphiphilic aggregates with a hydrodynamic diameter of 16 ± 10 nm in the solution. Hydrophilic PEG segments in the backbone structure and amino groups in the side chains are exposed to the water phase, and the siloxane backbone constitutes the central hydrophobic core of the aggregate. The surface amino groups exposed to water are positively charged, and the aggregates adsorb onto the negatively charged mica surface. A continuous adsorbed layer is formed on the mica surface, followed by the gradual deposition of aggregates on the top of the adsorbed layers. The adsorption behavior in this study qualitatively exhibits the same trend. The AFM images shown in Fig. 3 indicate a sea-island structure for the three concentrations. The images

of 0.005 wt% (Fig. 3a and inset) show the immediate adsorption of BIPA that leads to the formation of a uniform adsorbed layer ("sea" structure), followed by the gradual formation of an "island" on the top of the adsorbed layer. For the 0.05 and 0.5 wt% solutions, the images obtained immediately after sample preparation already have a sea-island structure (Fig. 3b, c), indicative of more rapid BIPA adsorption/deposition for larger concentrations. The largest island size and "connected" structure formation (inset of Fig. 3c) for 0.5 wt% are possibly not only due to the largest deposition speed but also due to the largest aggregate size in the solution (unfortunately, we could not perform DLS analysis for the 0.5 wt% solution because the solution was cloudy).

The results of the normal force measurements shown in Fig. 4 and Table 1 correspond well to the AFM observations. For the 0.005 wt% sample, the distance where repulsion starts is approximately the same as the hard-wall thickness (≈ 4 nm), which is almost double the adsorbed layer thickness obtained by AFM (1.9 nm, Fig. 3a). This is consistent with the uniform adsorbed layer formation with a small number of islands seen in Fig. 3a. The distance where repulsion starts is larger for higher concentrations (0.05 and 0.5 wt%), indicative of the trapping of deposited BIPA aggregates between opposed mica surfaces during surface approach. This also matches the AFM images (Fig. 3b, c), which show the deposited aggregates (island structure) on the adsorbed layer; a larger island size for higher concentrations is parallel with steric repulsion at larger surface distances. The trapped aggregates are gradually expelled from the gap between the mica surfaces during compression; the hard-wall thickness was below 5.6 nm for the three concentrations.

The dynamic thickness shown in Fig. 5 suggests further squeezing and/or conformational rearrangements of the BIPA molecules at the sliding interface; the minimum dynamic thickness was 2.7 nm or below. Estimation from the thicknesses reveals that the sliding films consist of two adsorbed BIPA layers on opposed mica surfaces that are compressed, flattened and shear aligned by applied load and sliding motions (each layer thickness of near 1.3 nm). The BIPA molecule has hydrophilic and hydrophobic moieties; the surface of the adsorbed layer adjacent to the mica and the opposed adsorbed layer should be constituted mainly by hydrophilic PEG segments and amino groups whose thicknesses are ~0.3 nm [33]. The width of the siloxane backbone, which constitutes the hydrophobic core, is ~0.7 nm [33, 37–39]. Then, simple addition gives the width (thickness) of the adsorbed layer of ~1.3 nm, which is in excellent agreement with the dynamic thickness. Some water molecules (diameter of ~0.25 nm) should also be trapped at the interface, so the true thickness of the adsorbed molecules may be thinner. This is possibly achieved by the

Table 3 Comparison of the friction behaviors between different concentrations

BIPA concentrations	0.005 and 0.05 wt%	0.5 wt%
Effect of pressure P on dynamic thickness D (Fig. 5b)	D not very dependent on P	D decreases with P
Effect of P on shear stress S (Fig. 7b)	S not very dependent on P (μ in Eq. 2 ≈0)	Large S at large P (finite μ in Eq. 2)
Effect of load L on contact area A (Fig. 8)	L primarily increases A ($A \propto L^{2/3}$)	A generally smaller than thinner concentrations, L primarily increases P
Contact geometry (contact fringe shape)	JKR-like contact Flat contact interface with a sharp edge around the corner	Hertz-like contact Rounded contact interface (thickness minimum at the center)
Pull-off force at separation	Detected	Not detected
Friction mechanisms	Adhesion-controlled friction	Load-controlled friction

further conformational rearrangements (flattening) of the PEG and siloxane backbones due to the high rotational freedom of ether bonds in the structures.

The thin BIPA films at three different concentrations exhibit extremely low friction; the friction coefficients μ were within the range of $4–7 \times 10^{-5}$ (Table 2). This excellent lubricity of course comes from the hydration lubrication mechanism [8, 16, 33]. There should be water molecules hydrated onto the amino groups and PEG segments at the surface of the adsorbed layers that generate hydration repulsion to support the applied load. The thickness of the intervening water between the adsorbed layers should be a monomolecular layer at most, deduced from the dynamic thickness (less than 2.7 nm). The high fluidity of the water molecules in the hydration layer realizes totally fluid-like properties at the sliding interface that gives rise to extremely low friction [8, 33].

We should note some differences in the adsorbed film structures (AFM observation) and friction properties (SFA results) between this study and our previous work [33]. The 0.05 wt% solution was measured in both studies. The AFM image ~15 min after surface preparation shown in ref [33] exhibited an almost flat adsorbed layer with few islands, which seems different from Fig. 3b in this study (apparent sea-island structure is observed immediately after sample preparation). In addition, we reported a time-dependent increase in friction in ref. [33], which was not observed in this study. These differences probably come from the fact that the BIPA aggregates in the solution are not in stable equilibrium but kinetically frozen aggregates [40, 41]. The aggregation characteristics, such as aggregation number and size (diameter), should change with elapsed time from solution preparation to AFM/SFA experiments and were not the same between the two studies. Furthermore, the friction properties of molecularly confined films, particularly polymer systems, often exhibit a large dependence on experimental parameters and procedures, such as the surface approaching speed and previous history (memory effects) [1, 42].
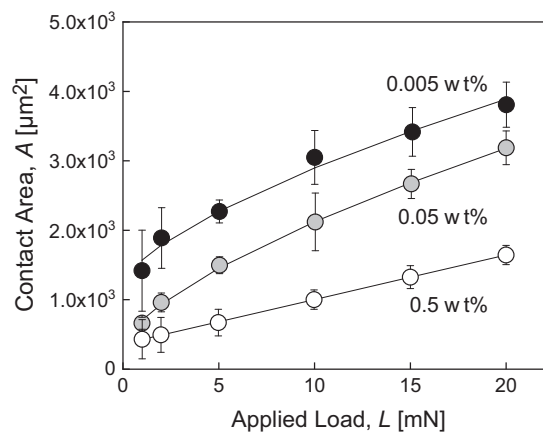

Fig. 8 Relationship between contact area A and applied load L for the three concentrations. The plots for 0.005 and 0.05 wt% are fit by $L^{2/3}$, and those for 0.5 wt% are fit by a linear function

Precise comparison between different concentrations

All three concentration solutions have two adsorbed layers at the sliding interface and exhibit extremely low friction. However, precise comparison implies slightly different features between different concentrations and will be discussed here. The observed friction behaviors are roughly divided into two groups and which are summarized in Table 3. For the 0.005 and 0.05 wt% solutions, the major effect of applied load is increasing the contact area; the relationship between the contact area and applied load is approximately fit by $A \propto L^{2/3}$ (see Fig. 8). The friction force increases with load mainly due to the increase in the contact area, and the shear stress (Fig. 7b) is not very dependent on pressure (μ in Eq. 2 ≈0); friction is governed by the adhesive interaction at the contact interface (S_0 in Eq. 2) [1, 2]. This interpretation is consistent with the JKR-like contact geometry [1, 43]; the FECO fringe for 0.005 wt% in Fig. 7b shows a flat contact interface with a sharp edge around the corner of the

contact area (indicative of a negative pressure at the edge). In addition, a pull-off force was detected upon separating the surfaces after friction measurements (typically ~4 mN or less). These analyses lead to the conclusion that the friction behavior of the 0.005 and 0.05 wt% solutions is typical "adhesion-controlled" friction (friction is governed by the adhesive interactions between surfaces rather than applied load) [1, 2].

The friction for the 0.5 wt% solution exhibits different behavior. The amount of the contact area that increases with the applied load is relatively small (Fig. 8). The major effect of the applied load is increasing the applied pressure, which results in a large decrease in the dynamic thickness (Fig. 5b). We cannot clearly see the effect of pressure on the shear stress in Fig. 7b due to the limited number of data points, but a positive dependence of the shear stress on pressure (finite μ in Eq. 2) is expected (as previously mentioned). These findings imply "load-controlled" friction (friction is governed mainly by applied load) [1, 2], which is supported by the Hertzian-type contact geometry (rounded fringe shape in Fig. 7b). No pull-off force was detected when we separated the surfaces after friction measurements, which is in agreement with the discussion above.

Now, we discuss the plausible origin of the difference in the friction behaviors between BIPA concentrations summarized in Table 3. In our previous study on a BIPA solution with a concentration of 0.05 wt%, we did not take into account the effect of unimers in the solution on adsorbed layer formation [33]. However, for the 0.005 wt% solution, considering the effect of unimers on the layer formation gives us the idea to explain the observed differences listed in Table 3. The adsorption behavior seen for the 0.005 wt% solution (Fig. 3a) is apparently different from that of higher concentrations; rather slow adsorption (bare mica structure is seen at the initial stage of observation) and highly uniform and relatively flat surface structure ($R_z \approx 1.2$ nm) of the adsorbed layer. A mesh-like fine structure is seen only for this concentration. These results may be attributed to the contribution of BIPA unimers to adsorbed layer formation on mica. The AFM image of 0.5 wt% (Fig. 3c) suggests the immediate formation of a sea-island structure with an island size near 300 nm (or larger) at the initial stage of adsorbed film formation. The R_z of the dark "sea" region is approximately 2.2 nm, which is much larger than that of the adsorbed mesh-like layer for 0.005 wt%. This could imply the large contribution of aggregate adsorption to the formation of the continuous "sea" region (adsorbed layer on mica). For the 0.05 wt% solution (Fig. 3b), it is difficult to assert the contribution of unimer adsorption on adsorbed layer formation.

If the discussion described above is adequate, the structural difference and resulting differences in the friction properties could be explained from the following

perspective: different contributions of unimer/aggregate on the formation of the adsorbed layer adjacent to mica surfaces. At a low BIPA concentration (0.005 wt%), the adsorbed layer adjacent to the mica surface is formed mainly by the adsorption of unimers in the solution, which could give the adsorbed BIPA layer a relatively high molecular packing density. This leads to a flat and rigid (undeformable or solid-like) sliding interface, which is consistent with the friction features summarized in Table 3. A flat and rigid sliding layer is also suitable for extremely low friction because of the formation of a continuous slip plane of a high-fluidity water layer. Little energy dissipation within the layers is expected because of the rigidity, which is also ideal for low friction. On the other hand, for the 0.5 wt% solution, the adsorbed layer is formed mainly by the adsorption of BIPA aggregates. Then, the BIPA molecules in the adsorbed layer might be rather disordered and less densely packed; the molecules are deformed more easily by compression and sliding motions. This model is consistent with the large pressure dependence of the thickness (Fig. 5) and shear stress (Fig. 7) and the Hertzian-like contact character, as listed in Table 3. The shear stress is slightly larger for 0.5 wt% than that for 0.005 wt%, possibly because of the extra energy dissipation within the loosely packed or "disordered" adsorbed layer during sliding. It is difficult to give a definite discussion on the case of 0.05 wt%. However, the friction features are rather close to those of 0.005 wt%, as listed in Table 3, so the contribution of unimer adsorption on the formation of the adsorbed layer on mica could be expected.

Finally, we should comment on the effect of BIPA concentration on friction properties from a practical perspective. The BIPA molecules required for low boundary friction are two adsorbed layers; excessive molecules not adsorbed on mica surfaces are squeezed out from the contact interface and do not contribute to friction reduction. Furthermore, the adsorbed BIPA layer structure is relatively rigid (possibly having a high packing density) and exhibits little energy dissipation during frictional sliding for low-concentration solutions. Therefore, a relatively low BIPA concentration solution should be appropriate for designing low friction surfaces in practical use.

Conclusions

We have studied the adsorption of a silicone-based amphiphilic block copolymer, bis-isobutyl PEG-14/amodimethicone (BIPA), from its aqueous solution onto a mica surface and the resulting tribological properties. Normal force and friction measurements were made for the BIPA solutions with three concentrations (0.005, 0.05, and 0.5 wt%) using the surface forces apparatus. All three concentration

solutions constituted sliding films of two adsorbed BIPA molecular layers between mica surfaces, which have extremely low friction coefficients μ on the order of 10^{-5}. These low μ values are based on the hydration lubrication mechanism; slippage of the fluid-like water layer (possibly monomolecular layer) between the adsorbed BIPA layers gives rise to excellent lubricity. A precise comparison of the results between concentrations implies possible structural differences in the sliding films and friction properties. The adsorbed BIPA layer for the lowest concentration solution (0.005 wt%) may be formed mainly by unimer adsorption from the solution. The adsorbed layer has a relatively high BIPA molecule packing density, which induces highly uniform and rigid properties of the sliding film. The structural characteristics of this adsorbed layer are more suitable for low energy dissipation during sliding and low friction. The contribution of BIPA aggregates to the adsorbed layer formation for the 0.5 wt% solution could induce rather disordered molecular packing within the adsorbed BIPA layer, which is presumably the origin of extra energy dissipation during sliding and a slightly larger friction force.

Compliance with ethical standards

Conflict of interest The authors declare no competing interests.

Publisher's note Springer Nature remains neutral with regard to jurisdictional claims in published maps and institutional affiliations.

References

1. Israelachvili JN. Intermolecular and surface forces. 3rd ed. Amsterdam: Academic Press; 2011.
2. Israelachvili J, Berman AD. Surface forces and microrheology of molecularly thin liquid films. In: Bhushan, B, editor. CRC handbook of micro/nanotribology, 2nd ed. Boca Raton: CRC Press; 1999. Chapter 9, p. 371−432.
3. Klein J, Kumacheva E. Confinement-induced phase transitions in simple liquids. Science. 1995;269:816−9.
4. Granick S. Soft matter in a tight spot. Phys Today. 1999;52:26−31.
5. Yamada S. General shear-thinning dynamics of confined fluids. Tribol Lett. 2002;13:167−71.
6. Yamada S. Structural aging and stiction dynamics in confined liquid films. J Chem Phys. 2009;131:184708/1−184708/9.
7. Robbins MO, Muser MH. Computer simulations of friction, lubrication and wear. In: Bhushan B, editor. Modern tribology handbook. Boca Raton: CRC Press; 2001. Chapter 20, vol 1, p. 717−65.
8. Klein J. Hydration lubrication. Friction. 2013;1:1−23.
9. Dowson D, Wright V, Longfield MD. Human joint lubrication. Biomed Eng. 1969;4:160−5.
10. McCutchen CW. The frictional properties of animal joints. Wear. 1962;5:1−17.
11. Dowson D. New joints for the millennium: wear control in total replacement hip joints. Proc Inst Mech Eng H. 2001;215:335−58.
12. Gong JP. Friction and lubrication of hydrogels—its richness and complexity. Soft Matter. 2006;2:544−52.
13. Lee S, Spencer ND. Sweet, hairy, soft, and slippery. Science. 2008;319:575−6.
14. Briscoe WH, Titmuss S, Tiberg F, Thomas RK, McGillivray DJ, Klein J. Boundary lubrication under water. Nature. 2006;444:191−4.
15. Raviv U, Klein J. Fluidity of bound hydration layers. Science. 2002;297:1540−53.
16. Briscoe WH. Aqueous boundary lubrication: molecular mechanisms, design strategy, and terra incognita. Curr Opin Colloid Interface Sci. 2017;27:1−8.
17. Cotton FA, Wilkinson G. Advanced inorganic chemistry. New York: Wiley; 1998.
18. Ma L, Gaisinskaya-Kipnis A, Kampf N, Klein J. Origins of hydration lubrication. Nat Commun. 2015;6:6060.
19. Chai L, Klein J. Interactions between molecularly-smooth gold and mica surfaces across aqueous solutions. Langmuir. 2009;25:11533−40.
20. Raviv U, Giasson S, Kampf N, Gohy JF, Jérôme R, Klein J. Lubrication by charged polymers. Nature. 2003;425:163−5.
21. Chen M, Briscoe WH, Armes SP, Klein J. Lubrication at physiological pressures by polyzwitterionic brushes. Science. 2009;323:1698−701.
22. Spencer ND. Aqueous Lubrication with poly(ethylene glycol) brushes. Tribol Online. 2014;9:143−53.
23. Briscoe WH, Klein J. Friction and adhesion hysteresis between surfactant monolayers in water. J Adhes. 2007;83:705−22.
24. Sorkin R, Dror Y, Kampf N, Klein J. Mechanical stability and lubrication by phosphatidylcholine boundary layers in the vesicular and in the extended lamellar phases. Langmuir. 2014;30:5005−14.
25. Goldberg R, Schroeder A, Barenholz Y, Klein J. Boundary lubricants with exceptionally low friction coefficients based on 2D close-packed phosphatidylcholine liposomes. Adv Mater. 2011;23:3517−21.
26. Banquy X, Burdyńska J, Lee DW, Matyjaszewski K, Israelachvili J. Bioinspired bottle-brush polymer exhibits low friction and Amontons-like behavior. J Am Chem Soc. 2014;136:6199−202.
27. Sorkin R, Kampf N, Zhu L, Klein J. Hydration lubrication and shear-induced self-healing of lipid bilayer boundary lubricants in phosphatidylcholine dispersions. Soft Matter. 2016;12:2773−84.
28. Chai J, Klein J. Role of ion ligands in the attachment of poly (ethylene oxide) to a charged surfaces. J Am Chem Soc. 2005;127:1104−5.
29. Chawla K, Lee S, Lee BP, Dalsin JD, Messersmith PB, Spencer ND. A novel low-friction surface for biomedical applications: modification of poly(dimethylsiloxane) (PDMS) with poly-ethylene glycol (PEG)-DOPA-Lysine. J Biomed Mater Res A. 2009;90A:742−9.
30. Tadmor R, Chen N, Israelachvili J. Normal and shear forces between mica and model membrane surfaces with adsorbed hyaluronan. Macromolecules. 2003;36:9519−26.
31. Lee DW, Banquy X, Israelachvili JN. Stick-slip friction and wear of articular joints. Proc Natl Acad Sci USA. 2013;110:E567−E574.
32. Andresen Eguiluz RC, Cook SG, Brown CN, Wu F, Pacifici NJ, Bonassar LJ, et al. Fibronectin mediates enhanced wear protection of lubricin during shear. Biomacromolecules. 2015;16:2884−94.
33. Miyamoto T, Yamazaki N, Watanabe S, Yamada S. Aqueous lubrication with the molecularly confined films of silicone-based amphiphilic block copolymer aggregates. Langmuir. 2019;35:15784−94.

34. Miyamoto T, Yamazaki N, Tomotsuka A, Sasahara H, Watanabe S, Yamada S. Tribological properties between taut hair fibers in wet conditions: a new shampoo formulation for eliminating stick-slip friction. J Surf Deterg. 2021;24:501–10.

35. Israelachvili JN, McGuiggan PM. Adhesion and short-range forces between surfaces. Part I: New apparatus for surface force measurements. J Mater Res. 1990;5:2223–31.

36. Luengo G, Schmitt FJ, Hill R, Israelachvili J. Thin film rheology and tribology of confined polymer melts: contrast with bulk properties. Macromolecules. 1997;30:2482–94.

37. Horn RG, Israelachvili JN. Molecular organization and viscosity of a thin film of molten polymer between two surfaces as probed by force measurements. Macromolecules. 1988;21:2836–41.

38. Yamada S. Layering transitions and tribology of molecularly thin films of poly(dimethylsiloxane). Langmuir. 2003;19:7399–405.

39. Yamada S. Nanotribology of poly(dimethylsiloxane) melt confined between hydrophobic surfaces. Tribology Online. 2006;1:29–33.

40. Xu R, Winnik MA, Riess G, Chu B, Croucher MD. Micellization of polystyrene-poly(ethylene oxide) block copolymers in water. 5. A test of the star and mean-field models. Macromolecules. 1992; 25:644–52.

41. Nicolai T, Colombani O, Chassenieux C. Dynamic polymeric micelles versus frozen nanoparticles formed by block copolymers. Soft Matter. 2010;6:3111–8.

42. Zeng H, Maeda N, Chen N, Tirrell M, Israelachvili J. Adhesion and friction of polystyrene surfaces around Tg. Macromolecules. 2006;39:2350–63.

43. Benz M, Gutsmann T, Chen N, Tadmor R, Israelachvili J. Correlation of AFM and SFA measurements concerning the stability of supported lipid bilayers. Biophy J. 2004;86:870–9.